Applied Physics Letters

RESEARCH ARTICLE | MAY 16 2022

Direct bandgap GeSn nanowires enabled with ultrahigh tension from harnessing intrinsic compressive strain

Daniel Burt ; Hyo-Jun Joo ; Youngmin Kim; Yongduck Jung; Melvina Chen; Manlin Luo; Dong-Ho Kang; Simone Assali ; Lin Zhang; Bongkwon Son; Weijun Fan ; Oussama Moutanabbir; Zoran Ikonic; Chuan Seng Tan ; Yi-Chiau Huang; Donguk Nam

Check for updates

Appl. Phys. Lett. 120, 202103 (2022)
https://doi.org/10.1063/5.0087477

View Online
Export Citation

09 September 2024 01:26:26

Nanotechnology & Materials Science
Optics & Photonics
Impedance Analysis
Scanning Probe Microscopy
Sensors
Failure Analysis & Semiconductors

Unlock the Full Spectrum.
From DC to 8.5 GHz.
Your Application. Measured.
Find out more
Zurich Instruments

AIP Publishing

Applied Physics Letters ARTICLE scitation.org/journal/apl

Direct bandgap GeSn nanowires enabled with ultrahigh tension from harnessing intrinsic compressive strain

Cite as: Appl. Phys. Lett. **120**, 202103 (2022); doi: 10.1063/5.0087477
Submitted: 6 February 2022 · Accepted: 29 April 2022 ·
Published Online: 16 May 2022

View Online Export Citation CrossMark

Daniel Burt,[1] Hyo-Jun Joo,[1] Youngmin Kim,[1] Yongduck Jung,[1] Melvina Chen,[1] Manlin Luo,[1] Dong-Ho Kang,[2] Simone Assali,[3] Lin Zhang,[1] Bongkwon Son,[1] Weijun Fan,[1] Oussama Moutanabbir,[3] Zoran Ikonic,[4] Chuan Seng Tan,[1] Yi-Chiau Huang,[5] and Donguk Nam[1,a)]

AFFILIATIONS

[1]School of Electrical and Electronic Engineering, Nanyang Technological University, 50 Nanyang Avenue, Singapore 639798, Singapore
[2]School of Electrical Engineering and Computer Science, Gwangju Institute of Science and Technology, Gwangju 61005, Republic of Korea
[3]Department of Engineering Physics, École Polytechnique de Montréal, C.P. 6079, Succ. Centre-Ville, Montréal, Québec H3C 3A7, Canada
[4]School of Electronic and Electrical Engineering, University of Leeds, Leeds LS2 9JT, United Kingdom
[5]Applied Materials, Inc., Sunnyvale, California 95054-3299, USA

[a)]Author to whom correspondence should be addressed: dnam@ntu.edu.sg

ABSTRACT

GeSn alloys are a promising emerging complementary metal–oxide–semiconductor compatible technology for applications in photonics and electronics. However, the unavoidable intrinsic compressive strain introduced during epitaxial growth has prevented researchers from pushing the performance of GeSn devices to the limit and realizing real-world applications. In this paper, we present a straightforward geometric strain-inversion technique that harnesses the harmful compressive strain to achieve beneficial tensile strain in GeSn nanowires, drastically increasing the directness of the band structure. We achieve ∼2.67% uniaxial tensile strain in ∼120 nm wide nanowires, surpassing other values reported thus far. Unique pseudo-superlattices comprising of indirect and direct bandgap GeSn are demonstrated in a single material only by applying a periodic tensile strain. Improved directness in tensile-strained GeSn significantly enhances the photoluminescence by a factor of ∼2.5. This work represents a way to develop scalable band-engineered GeSn nanowire devices with lithographic design flexibility. This technique can be potentially applied to any layer with an intrinsic compressive strain, creating opportunities for unique tensile strained materials with diverse electronic and photonic applications.

Published under an exclusive license by AIP Publishing. https://doi.org/10.1063/5.0087477

Group IV light sources compatible with silicon (Si) chips have long been considered the "Holy Grail" for the realization of monolithic photonic-integrated circuits.[1] Among various material platforms, including Si nanocrystals[2,3] and heavily doped germanium (Ge),[4–6] band-engineered Ge attaining direct bandgap has recently attracted much attention as the strongest candidate to achieve fully practical room-temperature on-chip light sources.[7–17] Additionally, band-engineered Ge is being extensively explored for advanced electronic devices, such as field-effect transistors (FETs), due to enhanced carrier mobilities.[18]

The two leading avenues toward achieving band-engineered Ge are tensile strain[7–10] and tin (Sn) alloying,[11–17] each of which has been progressing separately from each other until recently. Following a couple of recent theoretical papers[19,20] predicting the benefit of combining the two separate methods for realizing direct bandgap group IV materials, two research groups recently obtained tensile-strained GeSn microstructures and demonstrated low-threshold lasing.[21,22] However, to date, achieving tensile strain in GeSn required overcoming the harmful intrinsic compressive strain by employing complex fabrication methods, thus limiting the compatibility to complementary

09 September 2024 01:26:26

Published under an exclusive license by AIP Publishing

metal–oxide–semiconductor (CMOS) processes and preventing practical applications.

Herein, we present a simple and scalable technique which, contrary to the status-quo, harnesses the traditionally detrimental compressive strain for generating tensile strain in GeSn nanowires. We demonstrated that indirect bandgap GeSn nanowires with a relatively low Sn content of ∼6 at. % can be converted into direct bandgap nanowires by inducing a record-high tensile strain of ∼2.67%. Our innovative structural design allows inversion of the intrinsic compressive strain in GeSn layers into high and localized tensile strains with arbitrary spatial profiles. For example, by tuning design parameters including nanowire shapes and dimensions during single-step lithography, both the profile and magnitude of tensile strain can be customized for each nanowire. Since tensile strain reduces the energy bandgap, the unique strain distribution in each nanowire leads to a precisely tailored energy band profile. By achieving a spatially periodic strain distribution in GeSn, we produce a single-material pseudo-superlattice comprising of indirect and direct bandgap GeSn without relying on the change of the material composition. Photoluminescence (PL) studies show that tensile-strained GeSn wires exhibit a 2.5× enhanced PL emission over unstrained wires, presenting clear evidence of an increased directness of the band structure for the tensile-strained GeSn wires.

The fundamental concept of the geometric strain inversion technique is schematically illustrated in Fig. 1. Our design features a top-down patterned GeSn nanowire (highlighted in red) attached on either side by interlocked pads (highlighted in dark and light blue). By producing a pushing force in the base of the interlocked pads (highlighted in dark blue), the endpoints of the pads (highlighted in light blue) are pushed in opposing directions, resulting in a pulling force on the nanowire. This pulling force introduces a significant uniaxial tensile strain in the GeSn nanowire resulting in the successful inversion of the intrinsic compressive strain. The white arrows in the schematic represent the direction of pushing in the interlocked pads, which help us to visualize how a pulling force is introduced to the nanowire. To create the pushing force in the interlocked pads, we harness the problematic compressive strain that is inevitably introduced during the GeSn growth.[23] Upon releasing the entire device by etching the underlying

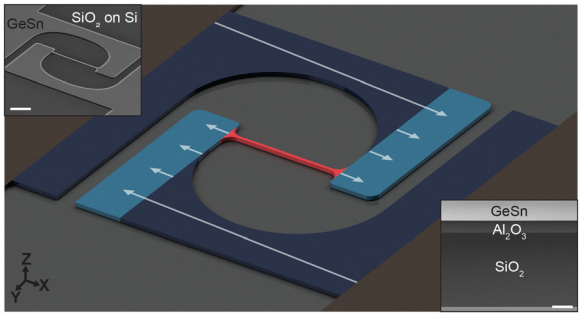

FIG. 1. Schematic illustration of our geometric strain inversion technique. Two interlocked pads (highlighted in dark and light blue) are pushed in opposing directions by releasing the intrinsic compressive strain, thus applying a pulling force and introducing a uniaxial tensile strain into the nanowire (highlighted in red). The white arrows aid the visualization of the push-to-pull principle. Top inset: SEM image of the fabricated nanowire. Scale bar, 5 μm. Bottom inset: cross-sectional TEM image of the GeSnOI substrate. Scale bar, 50 nm.

sacrificial layer, the compressive strain in GeSn causes the interlocked pads to expand in size, thus producing the pushing force along the white arrows. Previous works utilized the "push-to-pull" principle for scientific studies of mechanical properties of bottom-up nanomaterials.[24] However, the previous methodologies require complex sample preparation and external actuation from a micro-electromechanical system (MEMS) device, making them unsuitable for practical, integrated devices. In contrast, our innovative design only requires a simple patterning followed by the relaxation of the GeSn layer for inducing tensile strain in the nanowire, making our technique ideal for the realization of practical strain-engineered devices. Furthermore, the magnitude of the tensile strain in a nanowire with fixed dimensions can be conveniently tuned by changing the dimensions of the pads (i.e., the length), allowing for many nanowires with different strains to be fabricated in a single chip.

The top inset of Fig. 1 shows the scanning electron microscopy (SEM) image of a fabricated GeSn nanowire that is strained along the ⟨100⟩ direction. A coordinate system is shown at the left bottom to help visualize the direction of the uniaxial tensile strain, which is applied along the x-axis (ε_{xx}). The cross-sectional transmission electron microscopy (TEM) image (bottom inset of Fig. 1) reveals the layer structure of the high-quality GeSn-on-insulator (GeSnOI) substrate used in this study. High-resolution X-ray diffraction (HR-XRD) reciprocal space mapping was used to determine the Sn content and intrinsic biaxial compressive strain of the unpatterned GeSnOI layer, which was found to be 6.0 at. % and 0.1%, respectively (see the supplementary materials for detailed material characterization). The simple fabrication process involves only a single electron-beam lithography step followed by etching processes (see the supplementary material for the detailed fabrication procedure).

3D finite-element method (FEM) mechanical simulations were performed to confirm the validity of the fundamental principle of the geometric strain inversion technique. Figure 2(a) shows that a large uniaxial tensile strain can be induced in the nanowire while the residual compressive strain in the interlocked pads is fully released. The induced uniaxial strain is extremely uniform (<1% variation) across the entire volume of the nanowire, including an excellent uniformity across the thickness. Furthermore, FEM simulations show that strain can be easily increased only by increasing the length of the interlocked pads (see the supplementary material for the FEM simulations showing the effect of the pad length on the tensile strain).

The left panel of Fig. 2(b) shows the SEM image of a fabricated GeSn nanowire. The width and length of the nanowire are 300 nm and 7.5 μm, respectively, while the width and length of the pad are both 100 μm. Two-dimensional Raman mapping [the right panel of Fig. 2(b)] of this nanowire confirms a highly uniform strain distribution of ∼1.8% uniaxial tension along the ⟨100⟩ direction (see Methods in the supplementary material for more details on Raman spectroscopy). The result matches our FEM mechanical simulations and confirms the successful inversion of the intrinsic compressive strain into a uniaxial tensile strain. To investigate the effect of the nanowire dimension on pushing the achievable strain to the limit using our platform, we fabricated a large number of nanowires with varying geometrical dimensions simultaneously on a single chip. The GeSnOI substrate presented in this work is fabricated by epitaxy, direct bonding, mechanical lapping, and chemical-mechanical polishing (CMP).[25] More details on the GeSnOI substrate are presented in the

09 September 2024 01:26:26

Published under an exclusive license by AIP Publishing

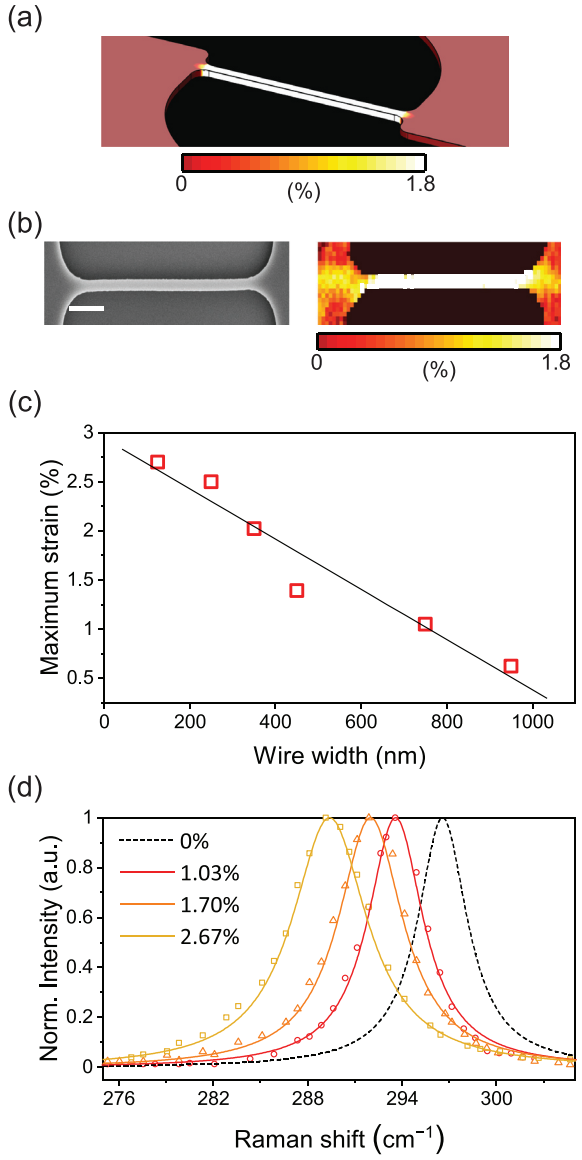

FIG. 2. (a) 3D FEM simulation of uniaxial strain of a nanowire, revealing excellent strain uniformity. Scale bar, 2.5 μm. (b) (Left) Top-view SEM image of a fabricated GeSn nanowire. Scale bar, 5 μm. (Right) 2D strain map measured by Raman spectroscopy revealing a highly uniform strain distribution over the entire area of the nanowire. (c) Maximum tensile strain measured in nanowires as a function of the wire width. The maximum value of experimentally achieved tensile strain increases with decreasing nanowire width. (d) Raman spectra of three GeSn nanowires with identical wire dimensions (the width and length are 120 nm and 5 μm, respectively) and increasing pad dimensions (75, 100, and 125 μm). The spectra of relaxed GeSn are plotted as a reference (black dashed line).

supplementary material. The GeSn nanowires were patterned using electron-beam lithography followed by reactive ion etching to transfer the pattern and wet/dry etching to release the GeSn structure. More details on the fabrication process can be found in the supplementary material. A 532-nm pump laser was used in conjunction with a micro-Raman spectroscopy experimental setup to measure the strain-induced shift of the Raman peak position. The Raman peak position was determined by Lorentzian fitting. The uniaxial tensile strain along the ⟨100⟩ direction is calculated using a strain-shift coefficient[26] of 269 cm^{-1}. Power dependent studies for GeSn were used to select an optical power that did not heat the nanowire, which can cause errors in strain measurements. 2D Raman mapping was performed to measure the strain distribution in the GeSn nanowires with a step size of 50 nm for the piezo-stage.

Figure 2(c) shows the maximum uniaxial tensile strain measured as a function of the nanowire width. The maximum value of experimentally achieved tensile strain increases with decreasing nanowire width. Reducing the nanowire volume (by reducing the width) increases the effective tensile strength due to a lower population of defects present, which allows for larger tensile strains to be realized.[27,28] A very high tensile strain of 2.67% was achieved in the smallest nanowire width (120 nm), and this value is the record-high achieved thus far for GeSn alloys, demonstrating the excellence of our geometric strain inversion technique. The maximum achieved strain is still lower than the theoretical limit of the tensile strength of Ge (14.6%),[29] possibly because of the increased defects when Sn is added into Ge.[23] Therefore, we expect that the tensile strain can be further increased by reducing the number of defects in GeSn during the low-temperature epitaxial growth, for example, by post-growth rapid thermal annealing (RTA).[30]

Figure 2(d) presents the Raman spectra measured for three nanowires with identical wire geometries (120 nm wide and 2.5 μm long) and increasing pad dimensions (75, 100, and 125 μm). All three nanowires show a clear redshift of the Raman peak position relative to the relaxed reference peak. The redshift of the Raman peak position (and, therefore, the tensile strain) becomes larger with increasing pad dimensions, verifying the ability of our strain inversion technique to tune the magnitude of the tensile strain by simply changing the design parameters. According to our band structure calculations using the **k·p** method, the amount of uniaxial tensile strain achieved in all three presented nanowires is sufficient to convert them from indirect to direct bandgap materials (see the supplementary material for more details on the band structure calculations).

To demonstrate the versatility of our strain inversion platform, we fabricated a unique pseudo-superlattice enabled in a single material without relying on the change of the material composition.[31] By producing a spatially periodic strain distribution in GeSn, we precisely tailor the energy band profiles in a single wire that achieves a periodically modulated indirect and direct bandgap GeSn pseudo-superlattice. Figure 3(a) presents the false-colored SEM image of the fabricated single-material pseudo-superlattice with repeating wider (blue color) and narrower (red color) regions. FEM simulations show that the periodic change of the wire width can lead to a periodically modulated strain distribution [Fig. 3(b)]. We fixed the nanowire length at 9 μm and introduced repeating narrower and wider regions with widths of 125 and 950 nm, respectively. The strain is significantly larger in the narrower regions due to a smaller cross section resulting in a greater force per area. Two-dimensional Raman mapping of the fabricated device provides experimental verification of the periodic strain [Fig. 3(c)], which is in excellent agreement with FEM mechanical simulations. The uniaxial tensile strain in the pseudo-superlattice has a maximum value of 1.4% in the narrower regions and a minimum value of 0.6% in the wider regions. We use the **k·p** method to convert

09 September 2024 01:26:26

Published under an exclusive license by AIP Publishing

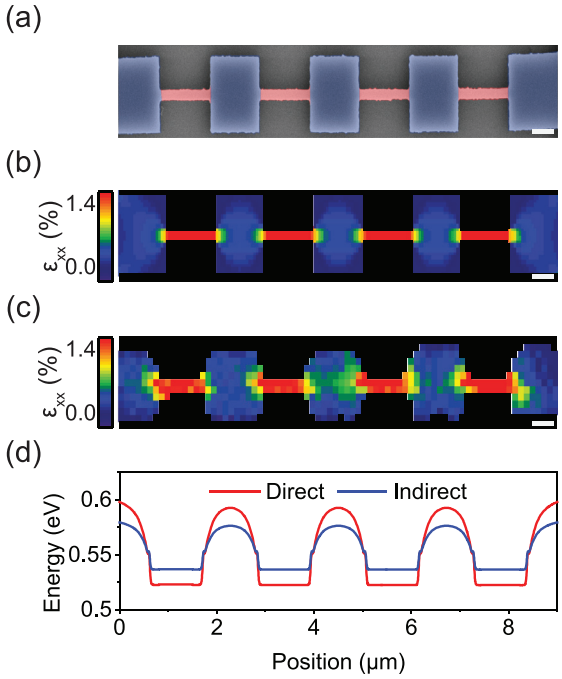

FIG. 3. A single-material pseudo-superlattice using periodically modulated strain. (a) False-colored SEM image of a fabricated strain pseudo-superlattice. The narrower regions are colored red, and the wider regions are colored blue. Scale bar, 250 nm. (b) Simulated 2D strain distributions revealing a periodic strain across the length of the strain pseudo-superlattice. The nanowire length is 9 μm, and the widths of the narrower and wider regions are 125 and 950 nm, respectively. Scale bar, 250 nm. (c) 2D strain distribution of the strain pseudo-superlattice from Raman spectroscopy. The uniaxial tensile strain has a maximum value of 1.4% in the narrower regions and a minimum value of 0.6% in the wider regions. Scale bar, 250 nm. (d) Direct and indirect bandgap energies across the length of the pseudo-superlattice, calculated using the **k·p** method. The narrower regions have become direct bandgap whereas the wider regions remain indirect bandgap, thus presenting the realization of a single-material pseudo-superlattice.

the simulated uniaxial tensile strain into direct and indirect bandgap energies as a function of the position in the pseudo-superlattice structure [Fig. 3(d)], revealing the periodic modulation of the bandgap energies. Interestingly, the narrower regions have sufficient tensile strain to convert the GeSn alloy into a direct bandgap material, while the wider regions remain an indirect bandgap material since the Sn alloy alone is insufficient to achieve direct bandgap in the GeSn layer used to produce the strain-induced pseudo-superlattice. Since the energy band profile of the single-material pseudo-superlattice can be modified by simply altering the shape and dimensions of the nanowire, our strain inversion technique is ideal for exploring the physics of pseudo-superlattices with highly customized energy band profiles and designing a variety of devices such as quantum cascade lasers[32] and multi-wavelength light sources.[33]

To study the influence of the tensile strain on the emission and further demonstrate the flexibility of our geometric strain inversion technique to be applied to as-grown substrates, we fabricated nanowires on an as-grown GeSn layer with a higher Sn content of 10.6 at. % (see the supplementary material for the details on the as-grown higher Sn content material). Samples were placed into a cryostat cooled to a temperature of 4 K. Nanowires were optically pumped by a pulsed laser with a wavelength of 1064-nm, a repetition rate of 1 MHz, and a pulse width of 5 ns. A 15× reflective objective lens was utilized to focus the pump laser onto the nanowires, resulting in a spot-size of ∼10 μm. The same reflective objective lens was used to collect the resulting PL signal, which was subsequently coupled into a Fourier transform infrared (FTIR) spectrometer, equipped with an InSb detector for detection.

Figure 4(a) presents PL spectra from relaxed and tensile strained nanowires. The measurement was conducted at 4 K, and a low pump power (<1 mW) was utilized to avoid any heating effects (see the supplementary material for the details of PL measurements). Broad spontaneous emission was observed from both the strained and relaxed nanowires, originating from the direct bandgap optical transition. The emission peak is redshifted by ∼200 nm upon the introduction of a uniaxial tensile strain due to the strain-induced bandgap narrowing.[34] Although we observed an experimental Raman shift of ∼1.5 cm^{-1} for the tensile strained nanowire (not shown here), there is currently no strain-shift coefficient for such a high Sn content layer to quantify the corresponding uniaxial strain. To estimate the value of the uniaxial strain using the emission peak position, we performed theoretical modeling for GeSn with a high Sn content of 10.6 at. %. Figure 4(b) shows the calculated direct bandgap emission wavelength as a function of uniaxial tensile strain. By comparing the measured emission peak position (2510 nm) against the simulated emission wavelengths for different tensile strain values, we extracted a uniaxial tensile strain of ∼0.75% for the strained nanowire.

In addition to the redshift, introducing a uniaxial tensile strain to the nanowire enhances the direct bandgap emission by a factor of ∼2.5. To understand the origin of this enhanced emission, we calculated the difference in energy between the L and Γ conduction band edge minima (i.e., the directness) [Fig. 4(c)]. As the uniaxial tensile strain increases, the energy difference between the L and Γ conduction valleys becomes larger, thus increasing the population of the Γ valley electrons that contribute to the direct radiative recombination (i.e., light emission). The enhanced light emission of the tensile strained wire demonstrates the excellent potential of our geometric strain inversion technique toward achieving an efficient group IV light source for CMOS-compatible optoelectronics.

In summary, we have presented a simple yet powerful method to harness the conventionally problematic intrinsic compressive strain for producing tensile-strained direct-bandgap GeSn. We achieved a record-high tensile strain of ∼2.67% and wavelength-tunable emission over a 200 nm range in nanowires that were fabricated with a single lithography step. We have demonstrated that our technique can be applied to both as-grown and bonded GeSn substrates. By precisely tailoring the spatial strain distribution in a single material, we produced strain-induced pseudo-superlattices that obtain the periodic modulation between indirect and direct bandgap materials. This way of creating pseudo-superlattices without relying on complex heteroepitaxy can be potentially employed for a class of quantum cascade lasers[32] and multi-wavelength light sources.[33] Our strain engineering platform lays the groundwork for creating various nanowires with unique functionalities including low-threshold nanowire lasing operating at different emission wavelengths and tunable photodetectors on a single chip. Another interesting range of applications of this geometric strain inversion technique is for electronic devices. Adding uniaxial

09 September 2024 01:26:26

Published under an exclusive license by AIP Publishing

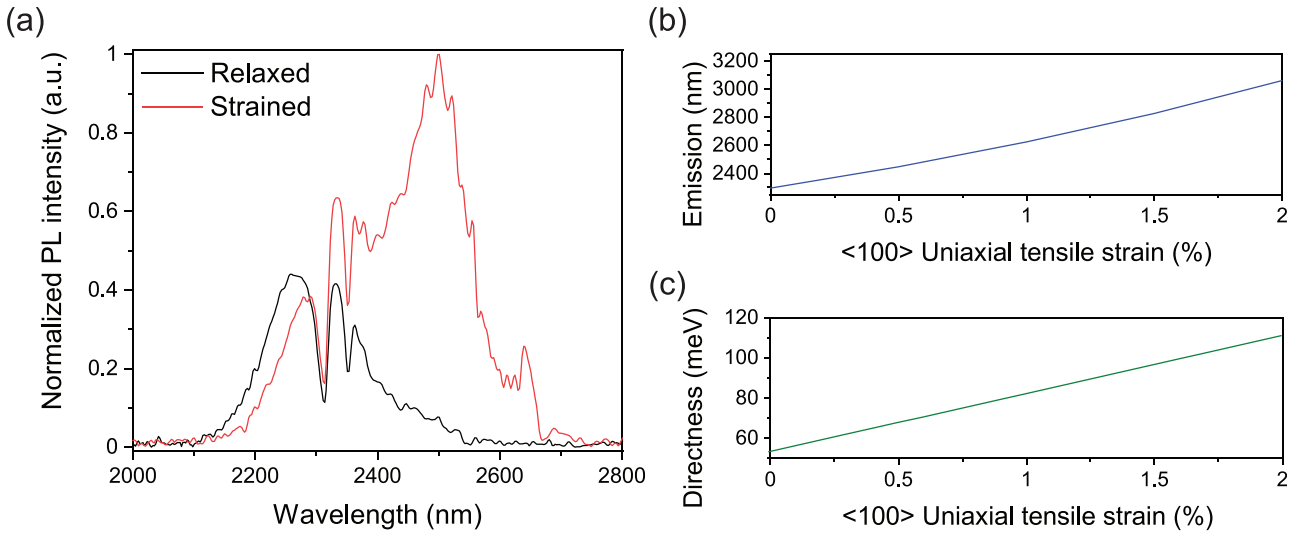

FIG. 4. Low-temperature photoluminescence of relaxed and strained nanowires. (a) Normalized emission spectra of relaxed and tensile strained nanowires with identical geometrical dimensions, showing broad spontaneous direct bandgap emission. The direct bandgap emission is redshifted by ∼200 nm while the intensity is increased by a factor of ∼2.5 for the tensile strained nanowire. (b) Calculated direct bandgap emission wavelengths as a function of uniaxial tensile strain. The experimental emission peak position of 2510 nm for the strained nanowire corresponds to a uniaxial tensile strain of 0.75%. (c) Calculated directness as a function of uniaxial tensile strain.

tensile strain using our geometric strain inversion method could enhance the electron mobility[35] to achieve improved GeSn nanowire nFETs. Our proposed technique can be applied to adjust materials' physical properties by creating nanostructures with variable tensile strain from any compressive-strained thin films. Our work presents a landscape of opportunities toward creating direct bandgap group IV nanowire devices.

See the supplementary material for XRD analysis of the GeSnOI substrate, more details on the bonding and fabrication, outline of the FEM simulations, details on the band structure calculations, and material characterization and SEM images of the higher Sn content as-grown layer.

The research of the project was in part supported by Ministry of Education, Singapore, under Grant No. AcRF TIER 1 (RG 115/21). The research of the project was also supported by Ministry of Education, Singapore, under Grant No. AcRF TIER 2 [MOE2018-T2-2-011 (S)]. This work was also supported by the National Research Foundation of Singapore through the Competitive Research Program (No. NRF-CRP19-2017-01). This work was also supported by the National Research Foundation of Singapore through the NRF-ANR Joint Grant (No. NRF2018-NRF-ANR009 TIGER). This work was also supported by the iGrant of Singapore A*STAR AME IRG (No. A2083c0053).

AUTHOR DECLARATIONS

Conflict of Interest

The authors have no conflicts to disclose.

Author Contributions

D.B., H.-J.J., and Y.K. contributed equally to this work.

DATA AVAILABILITY

The data that support the findings of this study are available from the corresponding author upon reasonable request.

REFERENCES

[1]Z. Zhou, B. Yin, and J. Michel, Light **4**, e358 (2015).
[2]L. Pavesi, L. Dal Negro, C. Mazzoleni, G. Franzò, and F. Priolo, Nature **408**, 440 (2000).
[3]S. G. Cloutier, P. A. Kossyrev, and J. Xu, Nat. Mater. **4**, 887 (2005).
[4]J. Liu, X. Sun, R. Camacho-Aguilera, L. C. Kimerling, and J. Michel, Opt. Lett. **35**, 679 (2010).
[5]R. E. Camacho-Aguilera, Y. Cai, N. Patel, J. T. Bessette, M. Romagnoli, L. C. Kimerling, and J. Michel, Opt. Express **20**, 11316 (2012).
[6]R. Koerner, M. Oehme, M. Gollhofer, M. Schmid, K. Kostecki, S. Bechler, D. Widmann, E. Kasper, and J. Schulze, Opt. Express **23**, 14815 (2015).
[7]J. Petykiewicz, D. Nam, D. S. Sukhdeo, S. Gupta, S. Buckley, A. Y. Piggott, J. Vučković, and K. C. Saraswat, Nano Lett. **16**, 2168 (2016).
[8]S. Bao, D. Kim, C. Onwukaeme, S. Gupta, K. Saraswat, K. H. Lee, Y. Kim, D. Min, Y. Jung, H. Qiu, H. Wang, E. A. Fitzgerald, C. S. Tan, and D. Nam, Nat. Commun. **8**, 1845 (2017).
[9]A. Elbaz, M. E. Kurdi, A. Aassime, S. Sauvage, X. Checoury, I. Sagnes, C. Baudot, F. Boeuf, and P. Boucaud, APL Photonics **3**, 106102 (2018).
[10]F. T. Armand Pilon, A. Lyasota, Y.-M. Niquet, V. Reboud, V. Calvo, N. Pauc, J. Widiez, C. Bonzon, J. M. Hartmann, A. Chelnokov, J. Faist, and H. Sigg, Nat. Commun. **10**, 2724 (2019).
[11]D. Stange, S. Wirths, R. Geiger, C. Schulte-Braucks, B. Marzban, N. von den Driesch, G. Mussler, T. Zabel, T. Stoica, J.-M. Hartmann, S. Mantl, Z. Ikonic, D. Grützmacher, H. Sigg, J. Witzens, and D. Buca, ACS Photonics **3**, 1279 (2016).
[12]J. Margetis, S. Al-Kabi, W. Du, W. Dou, Y. Zhou, T. Pham, P. Grant, S. Ghetmiri, A. Mosleh, B. Li, J. Liu, G. Sun, R. Soref, J. Tolle, M. Mortazavi, and S.-Q. Yu, ACS Photonics **5**, 827 (2018).
[13]Y. Zhou, W. Dou, W. Du, S. Ojo, H. Tran, S. A. Ghetmiri, J. Liu, G. Sun, R. Soref, J. Margetis, J. Tolle, B. Li, Z. Chen, M. Mortazavi, and S. Q. Yu, ACS Photonics **6**, 1434 (2019).
[14]V. Reboud, A. Gassenq, N. Pauc, J. Aubin, L. Milord, Q. M. Thai, M. Bertrand, K. Guilloy, D. Rouchon, J. Rothman, T. Zabel, F. Armand Pilon, H. Sigg, A. Chelnokov, J. M. Hartmann, and V. Calvo, Appl. Phys. Lett. **111**, 092101 (2017).

09 September 2024 01:26:26

Published under an exclusive license by AIP Publishing

[15]Q. M. Thai, N. Pauc, J. Aubin, M. Bertrand, J. Chrétien, V. Delaye, A. Chelnokov, J.-M. Hartmann, V. Reboud, and V. Calvo, Opt. Express **26**, 32500 (2018).
[16]Y. Kim, S. Assali, D. Burt, Y. Jung, H.-J. Joo, M. Chen, Z. Ikonic, O. Moutanabbir, and D. Nam, Adv. Opt. Mater. **10**, 2101213 (2021).
[17]H.-J. Joo, Y. Kim, D. Burt, Y. Jung, L. Zhang, M. Chen, S. J. Parluhutan, D.-H. Kang, C. Lee, S. Assali, Z. Ikonic, O. Moutanabbir, Y.-H. Cho, C. S. Tan, and D. Nam, Appl. Phys. Lett. **119**, 201101 (2021).
[18]S. Gupta, X. Gong, R. Zhang, Y. C. Yeo, S. Takagi, and K. C. Saraswat, MRS Bull. **39**, 678 (2014).
[19]S. Gupta, B. Magyari-Köpe, Y. Nishi, and K. C. Saraswat, J. Appl. Phys. **113**, 073707 (2013).
[20]D. Sukhdeo, Y. Kim, S. Gupta, K. Saraswat, B. Dutt, and D. Nam, IEEE Electron Device Lett. **37**, 1307 (2016).
[21]A. Elbaz, D. Buca, N. von den Driesch, K. Pantzas, G. Patriarche, N. Zerounian, E. Herth, X. Checoury, S. Sauvage, I. Sagnes, A. Foti, R. Ossikovski, J. M. Hartmann, F. Boeuf, Z. Ikonic, P. Boucaud, D. Grützmacher, and M. E. Kurdi, Nat. Photonics **14**, 375 (2020).
[22]J. Chrétien, N. Pauc, F. Armand Pilon, M. Bertrand, Q. M. Thai, L. Casiez, N. Bernier, H. Dansas, P. Gergaud, E. Delamadeleine, R. Khazaka, H. Sigg, J. Faist, A. Chelnokov, V. Reboud, J. M. Hartmann, and V. Calvo, ACS Photonics **6**, 2462 (2019).
[23]O. Moutanabbir, S. Assali, X. Gong, E. O'Reilly, C. A. Broderick, B. Marzban, J. Witzens, W. Du, S.-Q. Yu, A. Chelnokov, D. Buca, and D. Nam, Appl. Phys. Lett. **118**, 110502 (2021).
[24]H. Guo, K. Chen, Y. Oh, K. Wang, C. Dejoie, S. A. Syed Asif, O. L. Warren, Z. W. Shan, J. Wu, and A. M. Minor, Nano Lett. **11**, 3207 (2011).
[25]D. Burt, H.-J. Joo, Y. Jung, Y. Kim, M. Chen, Y.-C. Huang, and D. Nam, Opt. Express **29**, 28959 (2021).
[26]S. An, Y. C. Tai, K. C. Lee, S. H. Shin, H. H. Cheng, G. E. Chang, and M. Kim, Nanotechnology **32**, 355704 (2021).
[27]T. Zhu and J. Li, Prog. Mater. Sci. **55**, 710 (2010).
[28]D. S. Sukhdeo, D. Nam, J.-H. Kang, M. L. Brongersma, and K. C. Saraswat, Photonics Res. **2**, A8 (2014).
[29]L. T. Ngo, D. Almécija, J. E. Sader, B. Daly, N. Petkov, J. D. Holmes, D. Erts, and J. J. Boland, Nano Lett. **6**, 2964 (2006).
[30]Z. P. Zhang, Y. X. Song, Y. Y. Li, X. Y. Wu, Z. Y. S. Zhu, Y. Han, L. Y. Zhang, H. Huang, and S. M. Wang, AIP Adv. **7**, 105020 (2017).
[31]D. Nam, D. S. Sukhdeo, J. H. Kang, J. Petykiewicz, J. H. Lee, W. S. Jung, J. Vučković, M. L. Brongersma, and K. C. Saraswat, Nano Lett. **13**, 3118 (2013).
[32]J. Faist, F. Capasso, D. L. Sivco, C. Sirtori, A. L. Hutchinson, and A. Y. Cho, Science **264**, 553 (1994).
[33]P. Waltereit, O. Brandt, A. Trampert, H. Grahn, J. Menniger, M. Ramsteiner, M. Reiche, and K. Ploog, Nature **406**, 865 (2000).
[34]M. J. Süess, R. Geiger, R. A. Minamisawa, G. Schiefler, J. Frigerio, D. Chrastina, G. Isella, R. Spolenak, J. Faist, and H. Sigg, Nat. Photonics **7**, 466 (2013).
[35]Y. Chuang, C. Y. Liu, G. L. Luo, and J. Y. Li, IEEE Electron Device Lett. **42**, 10 (2021).

09 September 2024 01:26:26

Published under an exclusive license by AIP Publishing